UC Irvine
UC Irvine Electronic Theses and Dissertations

Title
Impact of Estrous Cycle on Cardiac Function

Permalink
https://escholarship.org/uc/item/22f4m2sf

Author
Nguyen, Thaotho Hoang

Publication Date
2024

Peer reviewed|Thesis/dissertation

eScholarship.org Powered by the California Digital Library
University of California

UNIVERSITY OF CALIFORNIA,
IRVINE

Impact of Estrous Cycle on Cardiac Function

THESIS

submitted in partial satisfaction of the requirements
for the degree of

MASTER OF SCIENCE

in Biomedical Engineering

by

Thaotho Hoang Nguyen

Thesis Committee:
Professor Naomi Chesler, Chair
Assistant Professor Pim Oomen
Assistant Professor Marcus Seldin

2024

© 2024 Thaotho Hoang Nguyen

TABLE OF CONTENTS

	Page
LIST OF FIGURES	iii
LIST OF TABLES	iv
ACKNOWLEDGEMENTS	v
ABSTRACT OF THE THESIS	vi
INTRODUCTION	1
CHAPTER 1: Estrous Cycle and Menstrual Cycle	
1.1 Introduction	2
1.2 Method	3
1.3 Results	6
1.4 Discussion	9
CHAPTER 2: Echocardiogram	
2.1 Introduction	10
2.2 Method	11
2.3 Results	14
2.4 Discussion	17
CHAPTER 3: Cardiac Function Changes throughout the Estrous Cycle	
3.1 Introduction	19
3.2 Method	20
3.3 Results	23
3.4 Discussion	29
CHAPTER 4: Conclusion	30
CHAPTER 5: Future Work	30
REFERENCES	32

LIST OF FIGURES

		Page
Figure 1	Estrous Observation Method	03
Figure 2	Vaginal Cytology Set Up	04
Figure 3	Flowchart of Submersion vs. Droplet Method	05
Figure 4	Staining of Submersion vs. Droplet Method	07
Figure 5	Comparing Vaginal Smears at Estrous Phases	08
Figure 6	Echocardiogram Set Up	12
Figure 7	Echocardiogram Images: Left Ventricle	15
Figure 8	Echocardiogram Images: Four Chamber	16
Figure 9	Echocardiogram Images: Pulmonary Artery and Aorta	17
Figure 10	Estrogen Level during Estrous and Menstrual Cycle	19
Figure 12	LabChart Data Analysis	23
Figure 12	Graphs of Fractional Shortening and Ejection Fraction	25
Figure 13	Graphs of Stroke Volume and Cardiac Output	25
Figure 14	Uterus Observation and % Uterus Weight: Body Weight	27

LIST OF TABLES

		Page
Table 1	Measurement Definitions	12
Table 2	Left Ventricle Calculation	13
Table 3	Left Ventricle Parameters	23
Table 4	Pulse Wave Doppler Parameters	25
Table 5	Non-Invasive Longitudinal Blood Pressure Measurements	25
Table 6	Terminal Point: body and heart chamber weight	27
Table 7	Invasive hemodynamic measurements	28

ACKNOWLEDGEMENTS

I am deeply grateful to my research advisor and committee chair, Dr. Naomi Chesler, for her unwavering guidance and mentorship throughout my graduate journey. Her insights and encouragement have been invaluable. I also extend my heartfelt thanks to my committee members, Dr. Pim Oomen and Dr. Marcus Seldin, whose constructive feedback and support were instrumental in shaping my thesis.

A special thanks is due to the members of the Chesler Lab and the Cardiovascular Innovation and Research Center. Your camaraderie and encouragement have greatly enriched my experience at the University of California, Irvine.

I would like to express my sincere appreciation to Dr. Tim Hacker, Dr. Cassandra K. Conway-O'Donnell, Dr. Mitchel Colebank, and Leticia Charco. Your expertise, support, and guidance have been critical throughout my master's program.

To my UCI friends, thank you for your constant support, humor, and motivation. Your presence has made this journey much brighter.

I am also grateful to my boyfriend for his unwavering support and for ensuring that I always had matcha on hand to fuel my studies.

I want to acknowledge my siblings—my sisters and brother-in-law—for their steadfast support and for always being there to keep me grounded when I needed it most.

Finally, I dedicate this thesis to my parents, MaiThảo Trương and Hiếu Nguyễn. Your love, support, and sacrifices have been the bedrock of my achievements. I am profoundly thankful for everything you have done for me and my siblings.
Con cảm ơn Ba Mẹ và con yêu Ba Mẹ nhiều lắm.

ABSTRACT OF THE THESIS

Impact of Estrous Cycle on Cardiac Function

by

Thaotho Hoang Nguyen

Master of Science in Biomedical Engineering

University of California, Irvine, 2024

Professor Naomi Chesler, Chair

Heart disease is the leading cause of death in the U.S. Premenopausal women generally have lower cardiovascular disease (CVD) rates compared to men, but after menopause, their risk exceeds that of men, largely due to decreased estrogen and progesterone levels. The exact effects of these hormones on cardiac function are still unclear. Our study examined the impact of the estrous cycle on cardiac function in C57BL/6 female mice to gain insights relevant to premenopausal women's heart health. To access the estrous cycle, we compared two protocols: visual assessment and vaginal cytology and found that vaginal cytology, being more quantitative and less biased, was to be the more reliable method. Among staining protocols, the droplet staining method effectively distinguished cell types and assessed estrous phases. For evaluating cardiac function, a protocol created and implemented for daily transthoracic echocardiography. This included methods for measuring left ventricle wall thickness, internal dimensions, ejection fraction, fractional shortening, and so much more. It was found that while heart rate remained stable throughout the cycle, stroke volume was higher in metestrus and diestrus phases, though not significantly. Notably, fractional shortening and ejection fraction were significantly lower when in diestrus compared to proestrus. This study underscores the importance of considering hormonal phase data in cardiovascular research.

INTRODUCTION

Heart disease is the leading cause of death across all genders and most racial and ethnic groups in the United States [1]. Historically, research on heart disease has often excluded females, leading to gaps in our understanding of physiological processes. It wasn't until 2014 that the National Institutes of Health (NIH) mandated the inclusion of both sexes in preclinical biomedical research involving cells and animals, unless specifically justified otherwise [2]. This policy shift has been echoed by many scientific journals, which are now adopting similar requirements [3].

The focus of my thesis is to develop and implement new protocols for assessing how the estrous cycle affects cardiac function in mice via echocardiogram. This research aims to enhance our understanding of heart function in women during the premenopausal phase. By elucidating how natural variations in sex hormones influence heart function, this work could provide valuable insights for cardiovascular research and help reduce data variability stemming from these hormonal fluctuations.

Chapter 1: Understanding and Identifying the Mice Estrous Cycle

1.1 Introduction

Identifying the stages of the estrous cycle is essential for understanding how this variable might impact key aspects of cardiovascular health [4, 5]. The estrous cycle, comparable to the human menstrual cycle, consists of four phases: proestrus, estrus, metestrus, and diestrus, and lasts approximately 4 to 5 days [6]. Numerous studies have explored different techniques for assessing the estrous cycle by examining changes in animal physiology and anatomy [4, 5]. These approaches encompass visual assessment, vaginal cytology, histological analysis of the reproductive organs, measurement of vaginal wall impedance and biochemical analysis of urine [7].

Microscopic analysis of vaginal smears has been a standard method for documenting the stages of the estrous cycle in laboratory rats and mice [8]. The vaginal mucosa, more specifically vaginal epithelium, undergoes changes in response to fluctuating estrogen levels during the estrous cycle [7]. By collecting cells through vaginal smears, researchers can identify the presence or absence of leukocytes, cornified epithelial cells, and nucleated epithelial cells at different phases of the estrous cycle [9].

In this chapter, we conducted a pilot study to implement two methods of identifying the estrous cycle: visual assessment and vaginal cytology. We also investigate the effectiveness of different staining techniques for vaginal cytology slides, specifically comparing the submersion method and the droplet staining method. This research advances the investigation by comparing methods for assessing estrous cycle timing and phases, thereby enabling researchers to incorporate this crucial variable into animal studies.

1.2 Methods

Animal Care

All animal procedures were approved by the University of California, Irvine Institutional Animal Care and Use Committee (IACUC). C57BL/6 mice were obtained from JAX Laboratories (Jackson Laboratories, Bar Harbor, ME). In total *n = 5* eight-week-old virgin female mice were housed in groups of five in micro-isolator cages on a 12-h light/dark cycle. Food and water were provided to mice *ad libitum*.

Visual Assessment Method

Estrous cycle phase was assessed visually by observing the color, moistness, and aperture of the vaginal opening [10, 11]. The animal was placed on a flat surface and the tail lifted to identify the vaginal opening and observe visual cues of the estrous phase such as color and wetness of the vaginal opening. Whereas proestrus (Fig 1A) is characterized by swollen, pink, and moist tissue, the vagina in estrus (1B) loses some pinkness and moistness but remains open. Metestrus (Fig 1C) can be identified by the slight closure of the vaginal canal, pale color, and presence of white cellular debris; in diestrus (Fig 1D) the vaginal canal is closed, has a pale color, no swelling, and no debris [10, 11].

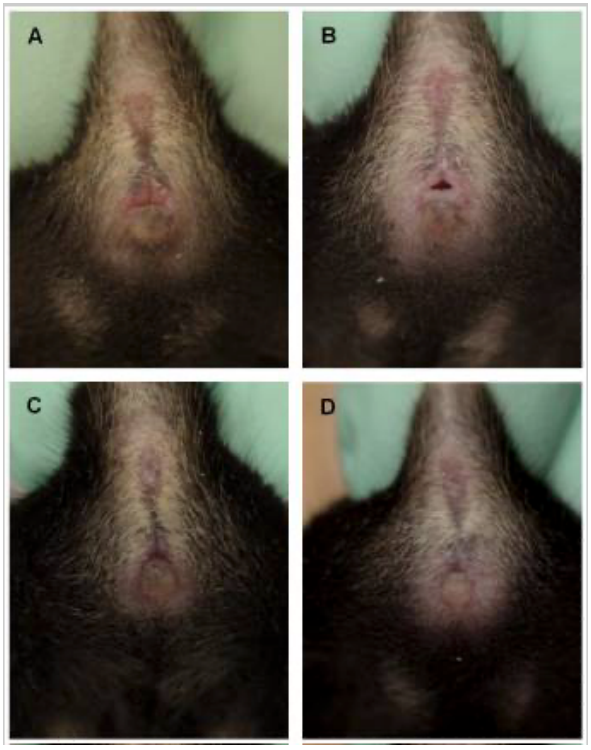


Figure 1: Observation Method images provided from Byers. 2012 A) Proestrus B) Estrus C) Metestrus D) Diestrus

Vaginal Cytology Method

Vaginal smears were collected at the same time daily for 5 consecutive days. The sterile swab previously soaked in sterile saline Dulbecco's Phosphate Buffered Saline (DPBS) (Dulbecco's Phosphate Buffered Saline - D8537, Sig ma Aldrich, St. Louis, MO, USA) (Fig 2) solution were gently inserted into the vagina with mouse in prone position. The swabs were not inserted further than 2mm (approximately the tip of the cotton swab) to prevent over stretching the vaginal wall or disturbing the cervix. Next, the swab was rotated 3 times to collect cellular debris and epithelial cells and were rolled on a clean slide and labeled appropriately. The slide was then allowed to airdry for 30 minutes and were fixed by submerging in methanol (99.8% Methanol, ThermoFisher Scientific A412-1) for 1 minute and air dried for another minute. Next the slides stained with either the submersion method or droplet method.



Figure 2: Vaginal Cytology Set Up (Created in BioRender)

Submersion Stain

Next, to stain for nuclei, the fixed slides were than dipped in Wright stain (Wright Stain, modified 0.3% (w/v), Sigma Aldrich, St. Louis, MO, USA) for 30 seconds before they were immediately washed with deionized (DI) water for 1 minute each (Fig 3A). Once a coverslip was placed, the slides were left to air dry at room temperature for 1-2 hours and stored in slide boxes until ready for imaging.

Droplet Stain

After fixing the slides, 10 drops of modified Wright stain (0.3% w/v, Sigma Aldrich, St. Louis, MO) were applied using a 3 mL graduated pipette (3.5 mL bulb draw, ensuring a drop size of 45 µL). The stain was allowed to sit for 1 minute before being carefully rinsed twice with deionized (DI) water, with each rinse lasting 1 minute (Fig 3B). Once a coverslip was placed, the slides were left to air dry at room temperature for 1-2 hours. The coverslips were then secured with clear nail polish to seal and preserve the samples. The slides were left to dry for an additional hour before being stored in slide boxes until ready for imaging.

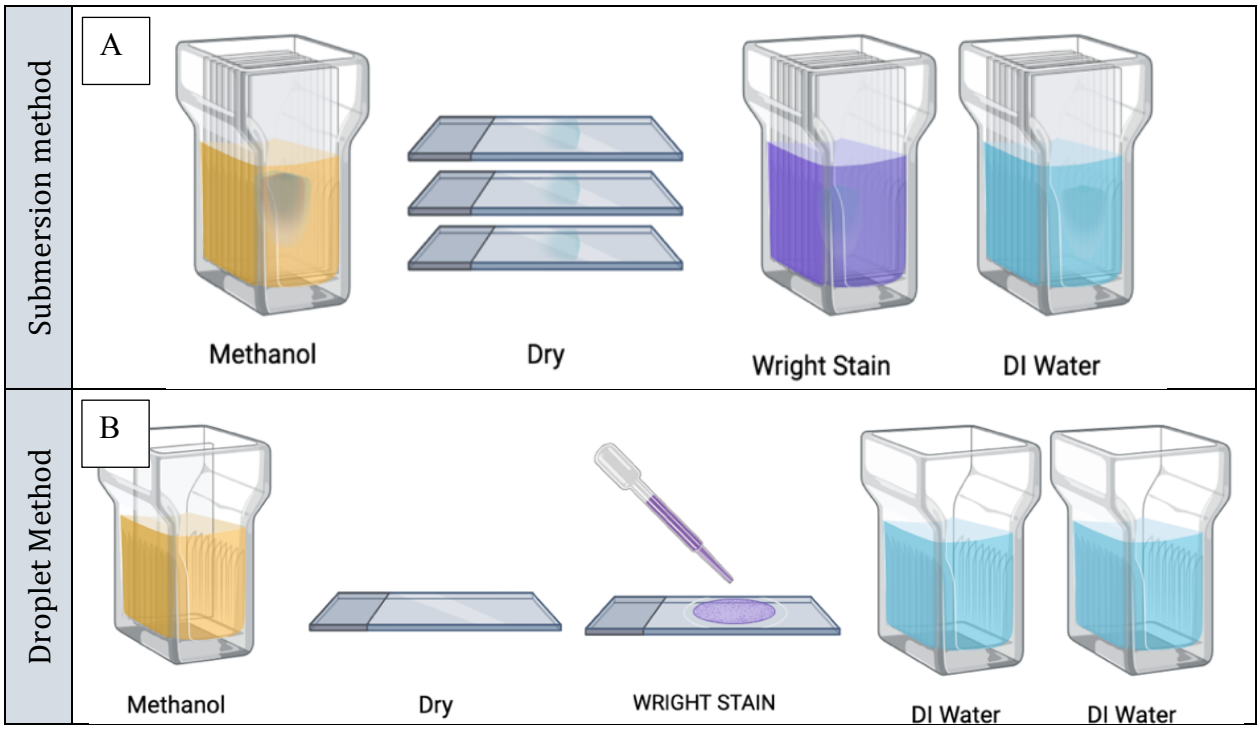


Figure 3: Flowchart of A) submersion method B) droplet method (Created in BioRender)

Imaging

The back of each slide was wiped with an alcohol pad to remove any debris before imaging. Images were subsequently taken using an Olympus BX43-Pol Microscope, an

Olympus DP23 Digital Camera, and cellSens^{TM} software (Olympus Corporation, Center Valley, PA, U.S.A.) at 4x, 10x, 20x, and 40x magnification.

1.3 Imaging Results:

Observations of the estrous cycle were conducted daily over a five-day period at the same time each day. However, distinguishing between proestrus and metestrus/diestrus phases using visual observation alone proved challenging. The method exhibited significant limitations, including potential bias if the researcher was aware of the previous data/phases. Additionally, the observations were highly qualitative and subjective, influenced by factors such as lighting conditions and personal judgment. The approach lacked quantitative precision, making it difficult to achieve consistent and objective assessments of the estrous cycle phases.

Figure 4 illustrates the comparison between the submersion and droplet staining techniques. The submersion method (Fig 4A) led to excessive background staining and insufficient staining of cell nuclei. This over-staining of the background made it difficult to discern individual cells and their types, resulting in a blurred and less informative image.

In contrast, the droplet staining method (Fig 4B) produced a more controlled and consistent application of stain, leading to clearer and more precise visualization of cell nuclei. This approach allowed for better differentiation between cell types and provided a cleaner background, enhancing the overall quality and interpretability of the slides.

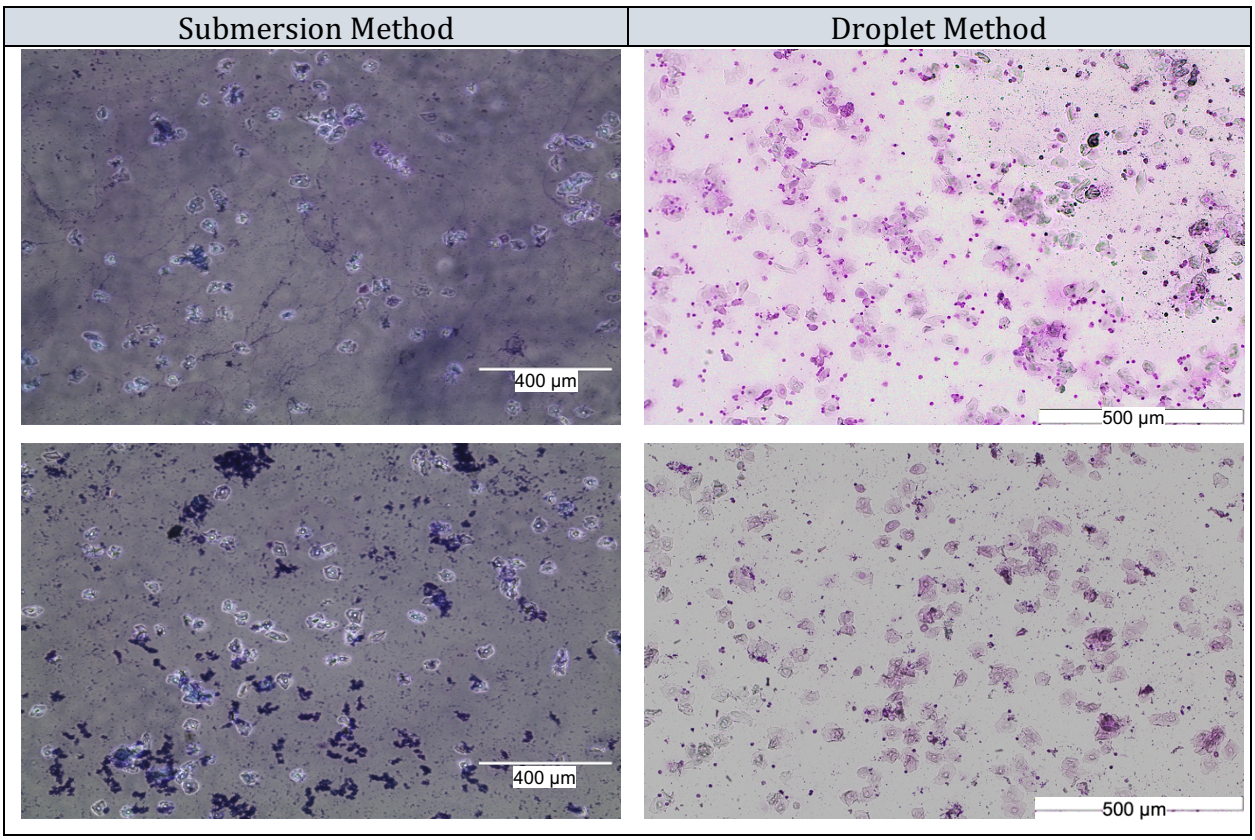


Figure 4: Submersion method, column on the left, led to excessive staining of the slides' background and insufficient staining of cell nuclei. Droplet staining method, column on the right, produced a more controlled and consistent application of stain.

Three main cell types are detected in vaginal smear samples: nucleated epithelial cells, cornified squamous epithelial cells, and leukocytes. The ratio of these cell types present in the smear can be used to identify mice in proestrus, estrus, metestrus, or diestrus. Proestrus (Fig 5A, 5B) is marked by a clear present nucleated cell, estrus (Fig 5C, 5D) by a predominance of cornified cells, metestrus (Fig 5E, 5F) by lightly stained cornified cells alongside a few leukocytes and nucleated cells, and lastly, diestrus (Fig 5G, 5H) by a higher number of leukocytes, some presents of nucleated and cornified cells, and generally lower cell counts. In late diestrus, the epithelial cells may become rounder or be organized in small clumps, indicating proestrus the next day; however, neutrophils will still be consistently observed. The ratio of these cells in vaginal secretions provide a basis for identifying the estrous cycle phase.

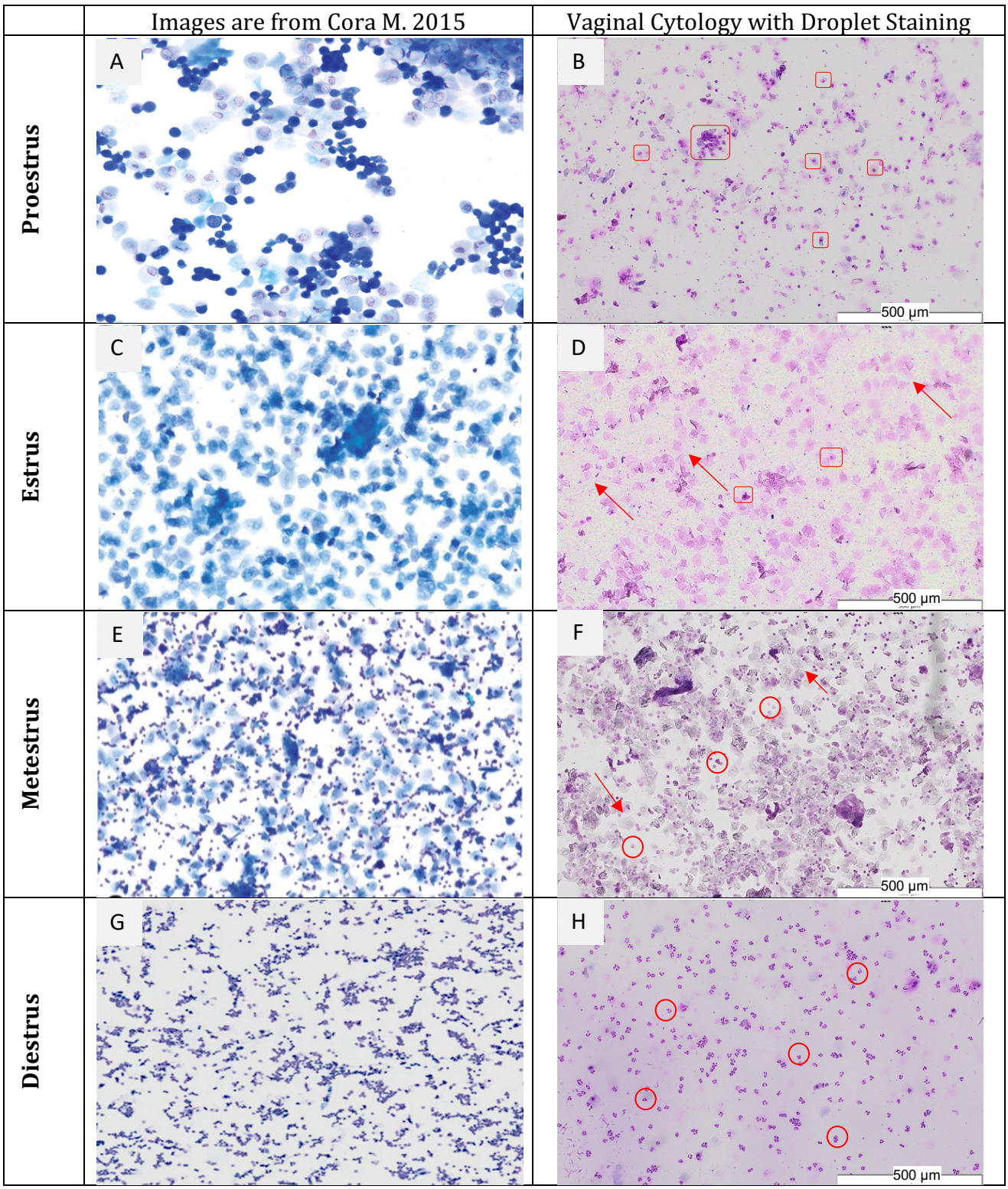


Figure 5:Comparing vaginal smears at proestrus (Fig 5A, 5B), estrus (Fig 5C, 5D), metestrus (Fig 5E, 5F), and late diestrus (Fig 5G, 5H) between images from Cora M. [8] and images from our pilot study. Phases are identified according to predominance of cell types identified: leukocytes (red circle), cornified epithelial (red arrow), or nucleated epithelial (red box).

1.4 Discussion

In this chapter, we investigated two methods of assessing the estrus phase of mice. Our experiments revealed that vaginal cytology, which is more quantitative and less biased than visual assessment, offers a more reliable means of identifying the stages of the estrous cycle. In addition, we compared two staining techniques—submersion and droplet staining methods – and found that the droplet staining method is superior for identifying the different types of cells shed throughout the estrous cycle and ultimately assess estrus cycle phase.

The droplet staining method provides an even and controlled application of the stain, resulting in clearer and more precise visualization of cell nuclei compared to the submersion method. The droplet method minimizes background staining and enhances the differentiation between cell types, leading to higher-quality and more interpretable results. Moving forward, we will adopt the droplet staining protocol for its improved consistency and effectiveness in vaginal cytology.

Chapter 2: Echocardiogram

2.1 – Introduction

Echocardiography (echo) stands out as a crucial non-invasive technique for visualizing cardiovascular structures and assessing cardiac function. Murine models have become increasingly used in cardiovascular disease research, largely due to the expanding availability of genetic models [12]. New advances in echocardiography technology have significantly enhanced spatial and temporal resolution, leading to more accurate evaluations of left ventricular systolic and diastolic function, as well as regional and vascular function [13]. This technique's versatility is evident in its application across various cardiovascular research contexts, including studies of mouse models with myocardial ischemia, and pulmonary hypertension [14].

This chapter will outline my implementation of transthoracic echocardiogram protocol for cardiovascular research in healthy C57BL/6 female mice, drawing on examples protocols from published literature on echocardiography [13]. This research aims to pave the way for future studies by integrating echocardiographic techniques into experimental frameworks.

2.2 - Method

Animal Care

All animal procedures were approved by the University of California, Irvine Institutional Animal Care and Use Committee (IACUC). C57BL/6 mice were obtained from JAX Laboratories (Jackson Laboratories, Bar Harbor, ME). In total *n = 5* eight-week-old virgin female mice were housed in groups of five in micro-isolator cages on a 12-h light/dark cycle. Food and water were provided to mice *ad libitum*.

Transthoracic Echocardiography

Daily transthoracic echocardiography using a Vevo F2 (FUJIFILM VisualSonics, Inc, Toronto, ON, Canada) ultrasound system was conducted to assess the morphology and function of the left ventricle, aorta, and pulmonary artery in a group of five (5) C57BL/6 female mice at 6-weeks-old using a 20-46 Mhz probe with a central frequency of 46MHz (UHF46x, FUJIFILM VisualSonics, Inc, Bothell, WA).

The mice were initially anesthetized with 5% isoflurane (Fluriso – Isoflurane USP, VET One, MWI Boise, ID) and maintained at 2% isoflurane and room air throughout the the entire procedure. The body temperature was maintained at 37°C using a heated- monitor platform (Mouse – Monitor Platform, FUJIFILM VisualSonics, Inc, Bothell, WA). Fur from the chest area was removed with Nair. Vevo Lab physiology monitor was used to record data like the electrocardiogram (ECG) electrodes, body temperature, and respiration. Signa gel electrode (Parker Laboratories, Fairfield, NJ) was applied as the conductive gel. Warmed ultrasound transmission gel (Parker Laboratories, Fairfield, NJ) was applied to improve the clarity of the sound waves transmitted from the ultrasound probe. Imaging was conducted daily at the same time and order for five consecutive days.

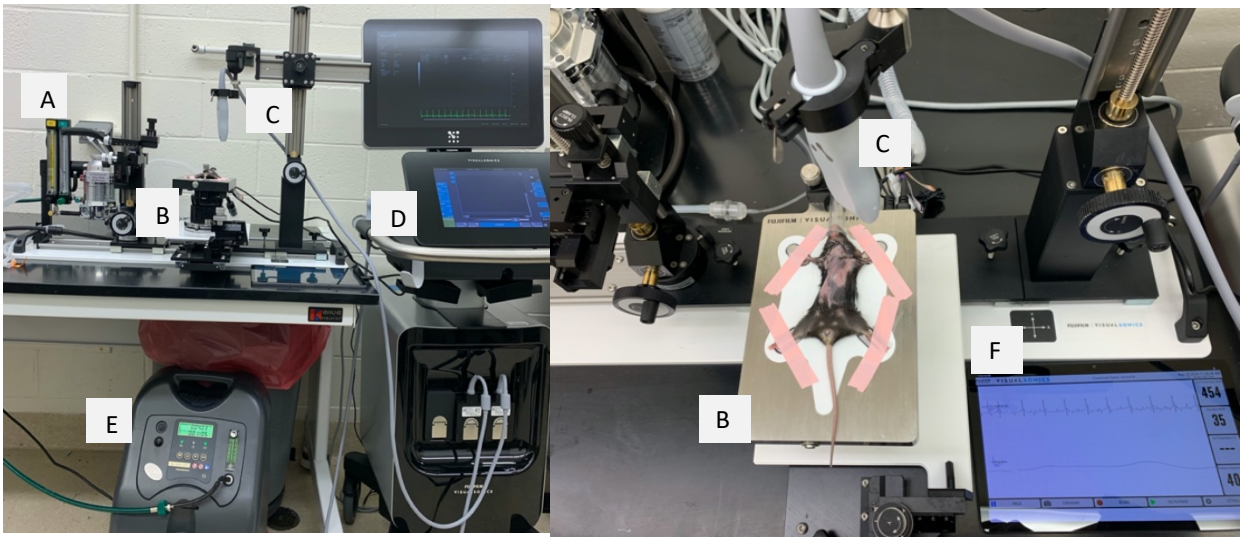


Figure 6: Echocardiogram set up A) Vevo Anesthesia System B) Animal platform (in both left and right image) C) Probe stand (in both left and right image) D) VevoF2 Machine E) Oxygen Concentrator F) physiology monitor

Measurements

Measurements were taken using B-mode, a two-dimensional imaging technique of the left ventricle (LV) long-axis. Additionally, M-mode at the LV papillary muscle level was also recorded for the quantification of cardiac dimensions and contractility. Pulse wave Doppler (PWD) were used to measure geometry and blood flow velocity in the aorta (Ao), pulmonary (PA) artery, mitral valve (MV), and tricuspid valve (TV). Images of four chamber view, PA, and Ao were also taken using color doppler mode.

Table 1: Measurements definitions

Parameters	
VTI	Velocity time interval
ET	Ejection time
AT	Acceleration time
IVCT	Isovolumic contraction time
IVRT	Isovolumic relaxation time

EF	Ejection fraction
FS	Fractional shortening
SV	Stroke volume
CO	Cardiac output
MPI	Myocardial Performance Index

Image Analysis

Vevolab v5.8.0 software was used to analyze the echocardiogram images. Echocardiographic parameters including left ventricle anterior wall (LVAW) and posterior wall (LVPW) thickness in systole and diastole, left ventricle internal dimensions (LVID) at diastole and systole (LVIDd and LVIDs respectively) were evaluated in M-mode by averaging measurements obtained over a minimum of three consecutive cardiac cycles. LV ejection fraction (EF), LV fractional shortening (FS), and LV posterior wall and anterior wall thickness (LVPW and LVAW) were calculated by using the imbedded formulas in Vevolab software (Table 2). The Myocardial Performance Index (MPI) is a calculation preformed on the Mitral Valve (MV) in PW Doppler spectrum used to assess both systolic and diastolic function of the left ventricle. EKG was also measured using surface electrodes and heart rate was determined with Vevolab software.

Table 2: Left Ventricle Calculation

	Formula
Left Ventricle Volume during systole	$LV\ Vol_d = LVID_d^3 \times (\frac{7.0}{2.4 + LVID_d})$
Left Ventricle Volume during diastole	$LV\ Vol_s = LVID_s^3 \times (\frac{7.0}{2.4 + LVID_s}$

Ejection Fraction (EF)	$EF\ (\%) = 100\ \times\ [\frac{LV\ Vol_d - LV\ Vol_s}{LV\ Vol_d}]$
Fractional Shortening (FS)	$FS(\%) = 100 \times\ [\frac{LVID_d - LVID_s}{LVID_d}]$
Myocardial Performance Index (MPI)	$MPI = [\frac{IVRT - IVCT}{AET}]$

2.4 – Results: Echocardiogram Image and image analysis

The echocardiographic analysis of the left ventricle (LV) in a healthy mouse revealed clear delineation of cardiac structures and function. The two-dimensional echocardiograms at end diastole and end systole (Fig.7) provided comprehensive views of the LV's dynamic changes throughout the cardiac cycle. The M-mode echocardiogram, obtained from the parasternal long-axis view, consistently measured the left ventricular anterior wall (LVAW) and posterior wall (LVPW) thicknesses, as well as the left ventricular inner diameter (LVID) in both systole and diastole.

In the assessment of mitral and tricuspid valve function (Fig.8), the B-mode image of the four-chamber view, supplemented with color Doppler mode, effectively visualized blood flow patterns. The red color indicated flow towards the probe through the mitral valve (MV) and tricuspid valve (TV). The Pulse wave Doppler (PWD) recording from the mitral valve leaflet provided detailed mitral inflow velocity patterns, including early diastolic (E wave) and late diastolic (A wave) velocities. Additionally, this recording allowed for the calculation of isovolumic contraction time (IVCT), isovolumic relaxation time (IVRT), and aortic ejection time (AET), all of which are important for characterizing diastolic function and filling pressures. The PWD data also revealed the E and A waves of the TV.

The examination of the pulmonary artery (PA) and aortic outflow (Ao) in a healthy mouse demonstrated clear imaging and flow assessment (Fig.9). The B-mode image of the PA and its color doppler mode counterpart, where blue indicated flow away from the probe, provided insights into the pulmonary circulation. Pulse Wave Doppler (PWD) of the PA complemented these observations with detailed velocity measurements. Similarly, the B-mode and color Doppler images of the Ao, with red indicating flow towards the probe, along with the PWD of the Ao, facilitated a thorough evaluation of aortic outflow dynamics. These images and Doppler recordings are integral for understanding both pulmonary and systemic circulatory function.

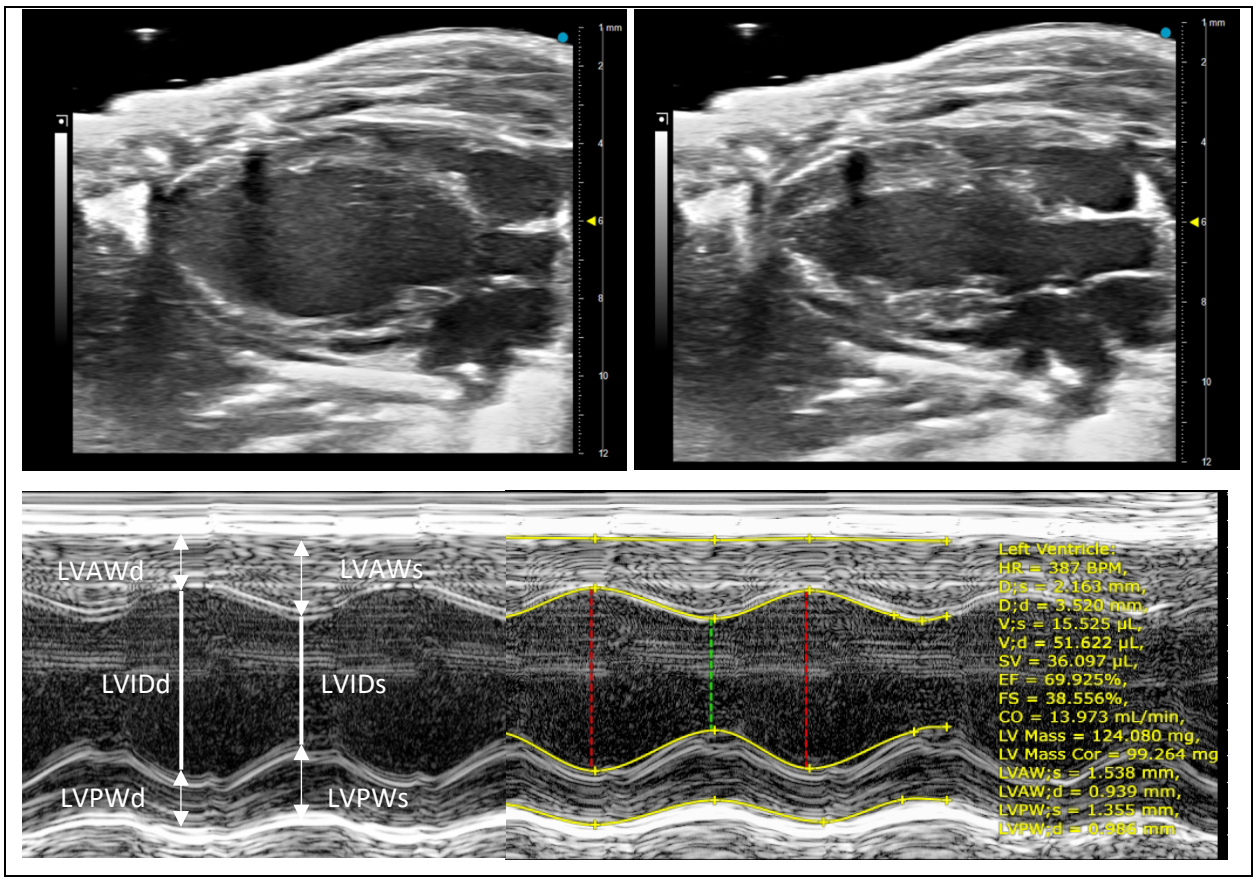


Figure 7: Representative echocardiogram of the LV in a healthy mouse. Two-dimensional echocardiogram: left, end diastole; right, end systole. Bottom, M-mode echocardiogram from the same mouse in the parasternal long-axis view. LVAW – left ventricle anterior wall (in systole or diastole), LVPW – left ventricle posterior wall (in systole or diastole), LVID – left ventricle inner diameter.

Four-Chamber – Tricuspid and Mitral Valve

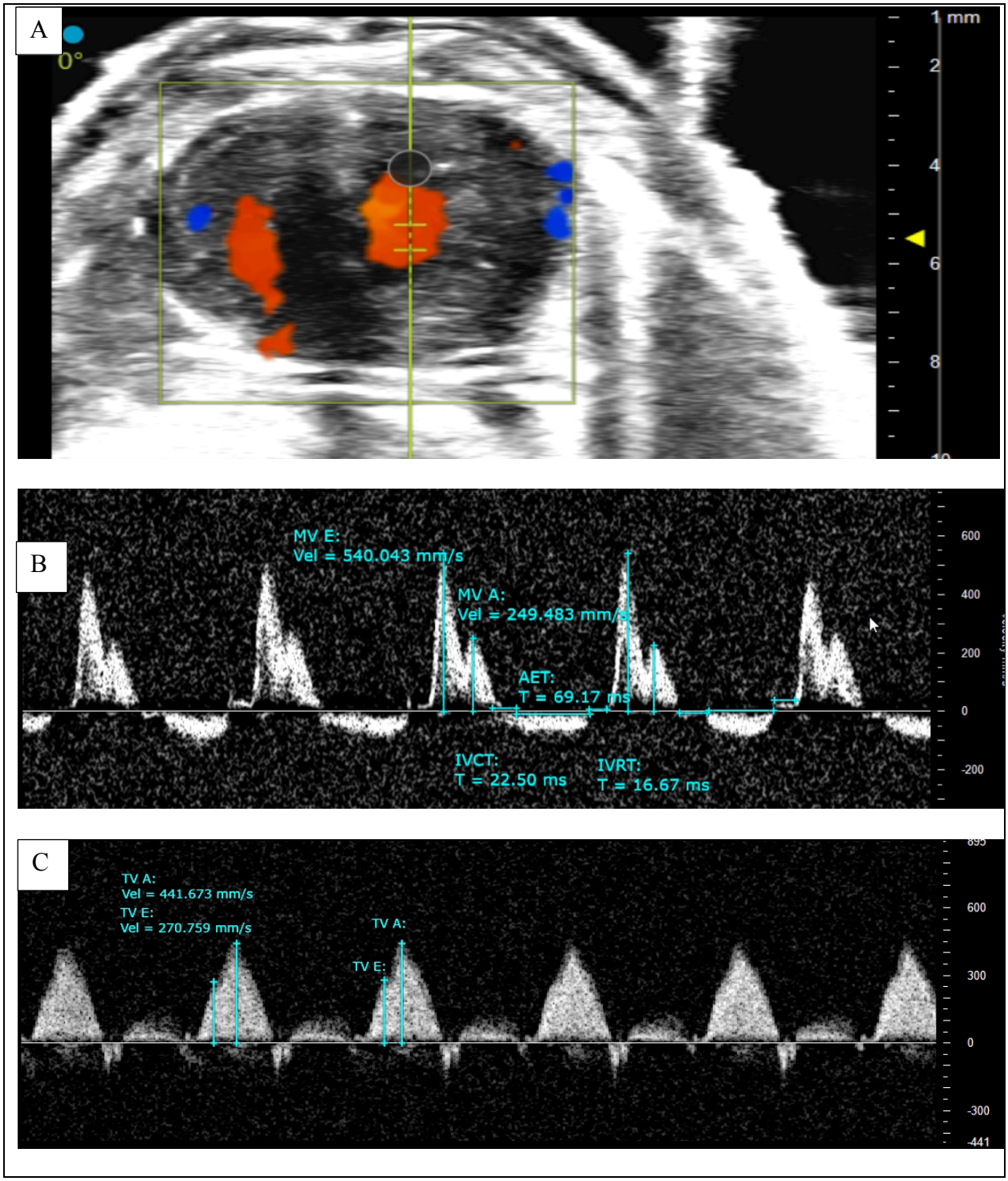


Figure 8: A) B-Mode of the four-chamber view with color doppler mode to help visualize the blood flow in tricuspid valve (TV) and mitral valve (MV), the red color indicates the flow toward the probe B) Pulse wave Doppler recording of mitral valve leaflet provides mitral inflow velocity patterns from which early diastolic velocity (E wave), late diastolic velocity with diastolic contraction (A wave). The IVCT – isovolumic contraction time and IVRT-isovolumic relaxation time is also a useful variable to characterize diastolic function and filling pressures. AET indicates aortic ejection time C) PWD of TV with E waves and A waves.

Pulmonary Artery and Aorta

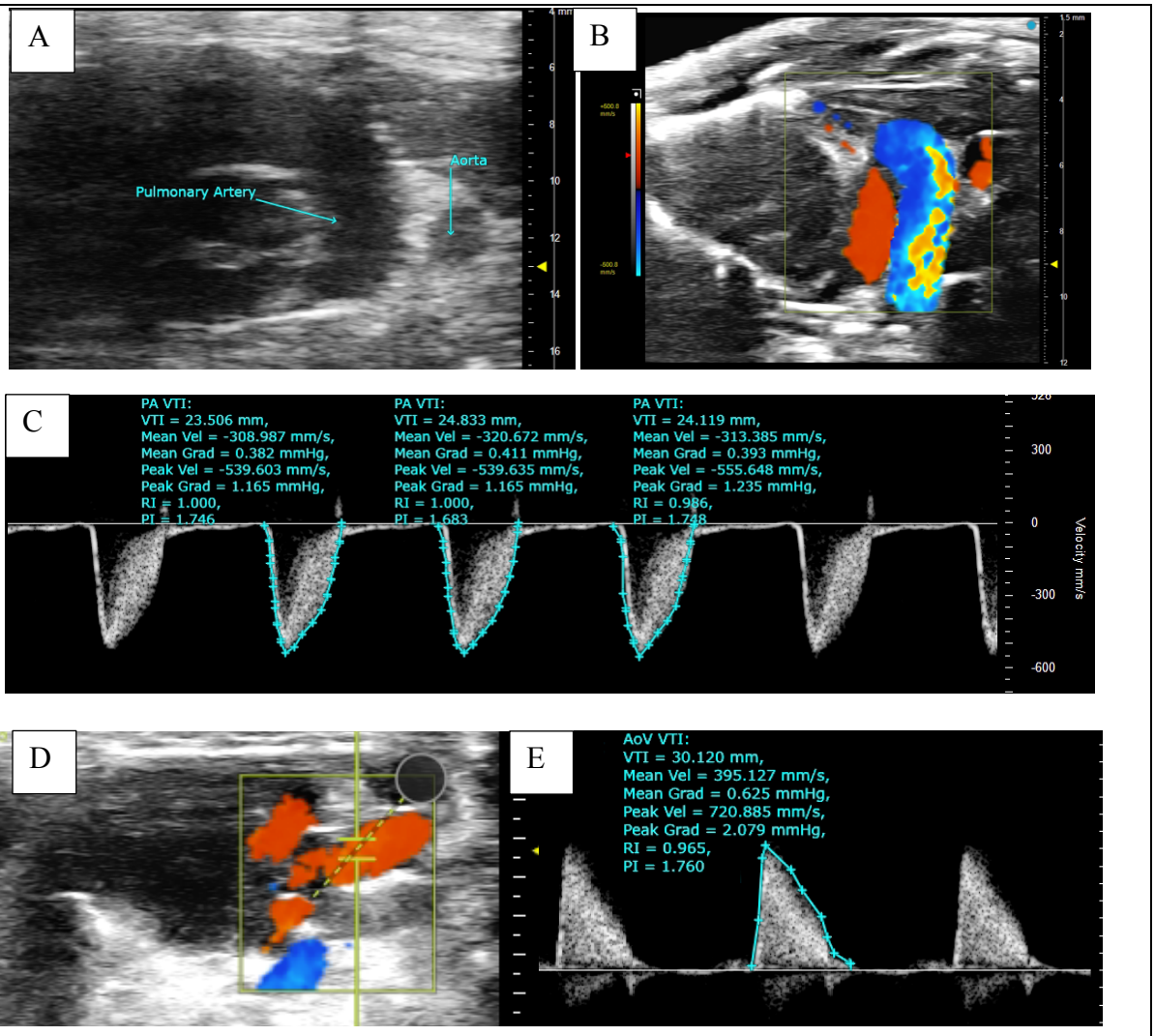


Figure 9: Representative echocardiogram of the pulmonary artery (PA) and the Aortic Outflow (Ao) in a healthy mouse. A) B-mode of the pulmonary artery; B) pulmonary artery captured with color doppler mode, the blue color indicates that the flow is flowing away from the probe C) Pulse wave Doppler of Pulmonary artery D) Ao captured with color doppler mode, the red color indicates that the flow is flowing toward from the probe E) Pulse wave Doppler of Ao.

2.4 - Discussion

In this chapter, I detailed the implementation of my approach for transthoracic echocardiogram protocol tailored for cardiovascular research using healthy C57BL/6 female mice. This protocol incorporates a range of echocardiographic techniques, including B-mode and M-mode imaging, Pulse wave Doppler (PWD), and color Doppler imaging, facilitated in

VevoF2. These methodologies were employed to meticulously evaluate various cardiac structural and functional parameters, such as left ventricular dimensions, wall thicknesses, and ejection fraction.

The implementation of the protocol for assessing cardiovascular health in C57BL/6 female mice has demonstrated its efficacy in providing detailed and reliable cardiac metrics. The integration of various echocardiographic techniques and the use of advanced software for image analysis contribute to a robust framework for cardiovascular research. This protocol enhances our understanding of cardiac function in murine models and lays the groundwork for future studies on cardiovascular diseases and therapies. It provides a basis for exploring pathological conditions, testing new murine models, and uncovering the mechanisms of cardiovascular function and dysfunction.

Chapter 3: Cardiac Function throughout the Estrous Cycle in Mice

3.1 - Introduction

Prior to menopause, females are less likely to develop overt cardiovascular disease (CVD) compared to age matched males [15]. However, post-menopause CVD onset increases substantially until the incidence of CVD in females surpasses that in males [16]. This disparity in heart disease is attributed to decreasing levels of estrogen and progesterone after menopause, however, the roles of female sex hormones in heart function premenopausally are not well understood.

Estrogen and progesterone cyclically rise and fall during the menstrual cycle with the highest amount of estrogen occurring immediately prior to ovulation and rising levels of progesterone occurring in the luteal phase (Fig 10) [17]. In women just prior to ovulation, systolic blood pressure and soft tissue compliance increases [18, 19]. In contrast, in women during the luteal phase, in which progesterone is rising and estrogen levels are falling, heart rate increases, and systolic blood pressure decreases [19].

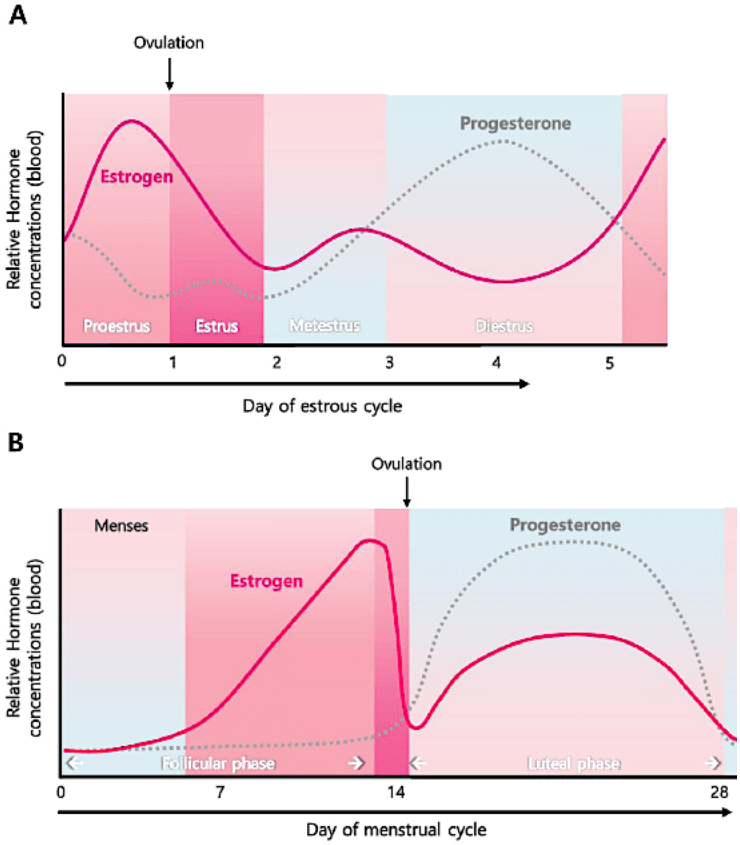


Figure 100: Images are from Hong K. 2020 - Estrogen level during estrous cycle and menstrual cycle (A) The estrous cycle is divided into four stages in mice: proestrus, estrus, metestrus, and diestrus. (B) The menstrual cycle is divided into two phases in humans: follicular phase and luteal phase

The 28-day (on average) human menstrual cycle and the 4-5 day (on average) mouse estrous cycle share some similarities. In both cases, the cycles consist of distinct phases. The mouse estrous cycle includes four phases: proestrus, estrus, metestrus, and diestrus. Proestrus is characterized by the preparation of the reproductive system for mating, similar to the human follicular phase. The estrus phase, often referred to as the "heat" period in animals, aligns with human ovulation when the egg is released. Metestrus and diestrus in mice correspond to the luteal phase in humans, involving changes in the uterus and hormonal fluctuations [11]. Understanding the impact of these cycles in mice is crucial for cardiovascular research using and can provide valuable insights into the effects of the menstrual cycle in women.

The goal of this study is to quantify the impact of the estrus cycle on cardiac function in mice to better design cardiovascular research studies using mice and understand the heart function of women in the premenopausal state. Knowledge of fluctuations in heart function that occur due to natural variations in sex hormones in females could help inform cardiovascular research and limit variability in data that results from those natural variations.

3.2 – Methods

Animal Care:

All animal procedures were approved by the University of California, Irvine Institutional Animal Care and Use Committee (IACUC). A total of n = 9 six-week-old virgin female mice obtained from JAX Laboratories (Jackson Laboratories, Bar Harbor, ME) were randomly housed in groups of five in micro-isolator cages on a 12-h light/dark cycle. Food and water were provided to mice *ad libitum*.

Estrous Cycle Identification

In pilot experiments, we found vaginal cytology was more consistent and effective for assessing estrus cycle stage than visual assessment. Therefore, to determine estrous stages, vaginal cytology was conducted using techniques described in chapter one. Vaginal smears were collected once daily between 9:30 am and 11:00 am for five consecutive days for two collection periods in 9 female mice. The slides were fixed with methanol and stained with Wright stain via droplet staining method. All images were imaged under an Olympus BX43-Pol Microscope, an Olympus DP23 Digital Camera, and cellSens^{TM} software (Olympus Corporation, Center Valley, PA, U.S.A.) at 4x, 10x, 20x, and 40x magnification.

Non-Invasive Blood Pressure

Hemodynamic parameters such as diastolic and systolic pressure, mean blood pressure, tail blood volume and flow were collected non-invasively from rodents using Kent Scientific's non-invasive blood pressure monitoring system. The noninvasive blood pressure measurement methodology consists of placing a cuff around the tail to occlude blood flow when inflated. Upon deflation, one of several types of noninvasive blood pressure sensors, placed distal to the occlusion cuff, can be used to monitor the blood pressure. Animals undergo a one-week acclimation period before testing in which they are placed in a restraint device for 15 minutes, once per day. Once acclimated, animals in the restraint are placed on a warming pad to allow tails to reach the optimal temperature of 32-35 °C. Animal temperature is monitored using a far-infrared thermometer.

Transthoracic Echocardiogram

Daily transthoracic echocardiography using a Vevo F2 ultrasound system was conducted for five days to assess the morphology and function of the left ventricle, aorta, and

pulmonary artery in a group of nine (9) C57BL/6 female mice at seven-weeks-old using a 20-46 Mhz probe with a central frequency of 46MHz (UHF46x, FUJIFILM VisualSonics). The mice were initially anesthetized with 5% isoflurane and maintained at 2% isoflurane during the entire procedure. A heated platform was used to maintain the body temperature at 37°C.

Imaging was conducted daily at the same time and for 5 consecutive days. B-mode and M-mode images were taken of the left ventricle. B-mode and Pulse wave Doppler (PWD) were used to measure geometry and blood flow velocity in the aorta (Ao) and pulmonary artery (PA).

Image Analysis

Image analysis was conducted the same way as described in chapter two on Vevolab v5.8.0 software. EF, FS, CO, and SV were calculated using echocardiographic parameters by measuring LVAW and LVPW thicknesses in both systole and diastole using M-mode.

Ventricular function and pressure flow measurement for left-sided measurements

After the two collection periods of echocardiogram and non-invasive blood pressure, invasive hemodynamic measurements were obtained in n = 5 during proestrus and n = 4 during diestrus. Anesthesia was induced with an intraperitoneal injection of urethane solution (1 mg/g body weight) to maintain heart rate in n = 9. Prior to thoracotomy, rodents are intubated with an 18 gauge and placed on the ventilator (Harvard Apparatus, Holliston, MA) at 120-150 breaths per minute with a stroke volume of about 150 microliters. A 1.0 to 2.0 Fr high fidelity pressure catheter (Millar, Houston, TX) was advanced into the left ventricle. After stabilization, left ventricular pressure data was recorded on commercially available software, LabChart (Fig 11) to assess the proper location for the catheter. Ventricle pressures, along with heart rate were continuously displayed, recorded and saved with

available software. After instrumentation is established, and initial pressure-volume measurements are taken, the vena cava was isolated and briefly occluded to obtain alterations in venous return for determination of end-systolic pressure (ESP) relations. Left ventricular pressure and volume were continuously recorded at 1000 samples/second.

LV mechanical function was assessed using established parameters including maximum and minimum pressure derivatives (dP/dt_{max}, dP/dt_{min}), and the slope of dP/dt_{max}-end diastolic volume (EDV) relationship obtained from inferior vena cava occlusions.

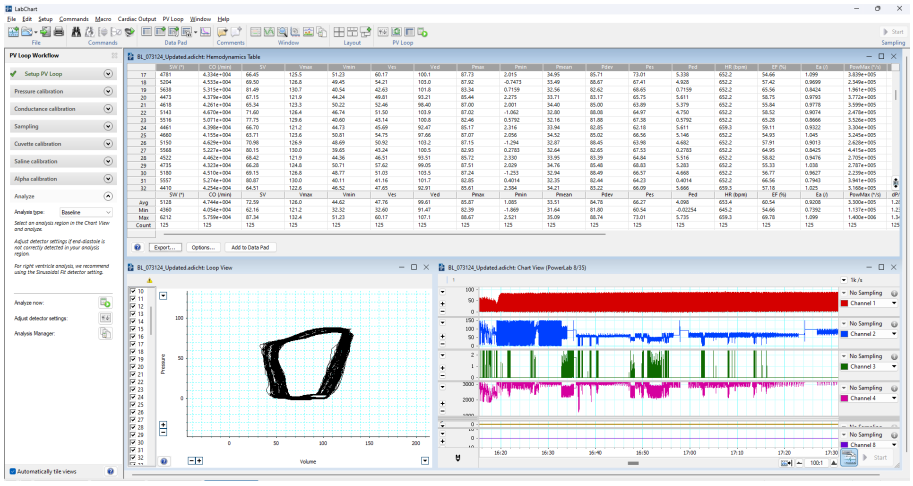


Figure 11: A view in Lab Chart of how data are analyzed.

Tissue Collection

After all measurements were complete, blood samples were taken, and serum was extracted. After euthanasia, the whole heart was weighed. The right ventricular free wall was removed and weighed as was the left ventricle (LV) plus septum (S).

Statistical Analysis

Measured parameters were categorized into one of the four stages of the estrous cycle as determined by vaginal cytology. All echocardiography data are provided as mean $\pm$ SD

with $n = 9$ samples except for metestrus ($n = 8$). A linear mixed effects model with animal-specific random effects for the intercept was used to evaluate intra-group comparisons with cycle phase. Multiple comparisons were conducted using the estimated marginal means of the main (fixed) effects using a Tukey-Kramer adjustment. We used a Kenward-Roger approximation for degrees of freedom to handle the missing imbalanced design in metestrus. Significant differences are denoted by * with a $p < 0.05$ threshold. All statistics were performed using R-Studio and graphed via GraphPad Prism.

3.3 - RESULTS

Longitudinal Measurements

As shown in table 3, heart rate (HR) did not vary over the course of the estrous cycle. Both fractional shortening (FS) and ejection fractioning (EF) showed a significant change with natural fluctuations in estrogen and progesterone in the female mice in this sample. FS and EF were significantly lower in mice in diestrus (p-value 0.004 and 0.0007) and metestrus (p-value 0.02 and 0.03) compared to mice in proestrus (Fig 12). Stroke volume (SV) was higher during metestrus compared to proestrus and estrus, but there was only a significant decrease when compared to diestrus. Cardiac output (CO), calculated as the product of HR and SV, was also significantly different between metestrus and diestrus with p-value 0.02 and 0.007 respectively.

Table 3: Left Ventricle Parameters

	Proestrus	Estrus	Metestrus	Diestrus
	n = 9	n = 9	n = 8	n = 9
Age (wk)	7 ± 3	7 ± 3	7 ± 3	7 ± 3
Heart Rate (BPM)	460.83 ± 32.77	482.70 ± 28.53	470.39 ± 55.05	466.03 ± 24.36
Stroke Volume (SV) (uL)	21.86 ± 7.19	21.54 ± 3.97	25.08 ± 4.08 *	19.33 ± 4.23 *

Cardiac Output (CO) (mL/min)	10.01 ± 1.76	10.39 ± 2.12	11.79 ± 2.32 **	8.93 ± 1.80 **
LVAWd	0.95 ± 0.15	0.95 ± 0.16	0.87 ± 0.19	0.87 ± 0.10
LVAWs	1.35 ± 0.19	1.38 ± 0.20	1.23 ± 0.19	1.17 ± 0.87
LVPWd	0.93 ± 0.17	0.90 ± 0.11	0.79 ± 0.17	0.93 ± 0.19
LVPWs	1.31 ± 0.22	1.29 ± 0.13	1.10 ± 0.12	1.20 ± 0.18

SV was higher during metestrus compared to proestrus and estrus, but there was only a significant decrease when compared to diestrus. CO was also significantly different between metestrus and diestrus. Values are *means ± SD* (*P < 0.05, **P < 0.001, and ***P < 0.0001).

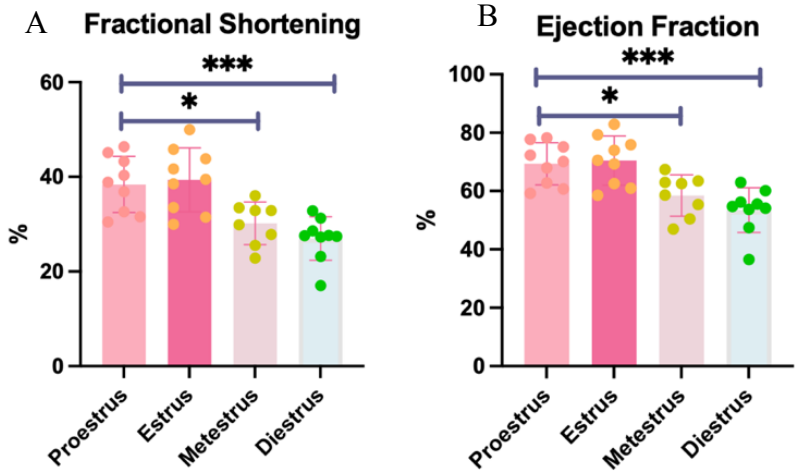
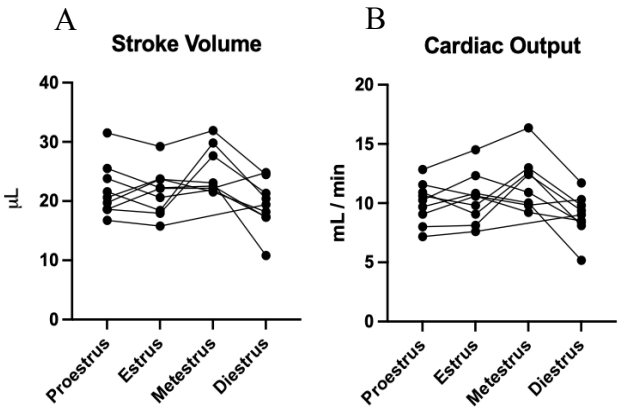


*Figure 12: Mice in diestrus exhibited a significant decrease in A) fractional shortening (FS) and B) ejection fraction (EF) in compared to mice in proestrus (*P < 0.05 and ***P < 0.0001).*

Graphs A and B in figure 13 illustrate the changes in stroke volume (SV) and cardiac output (CO) for each individual animal across the four phases of the estrous cycle.

Figure 13: Graphs A and B illustrate the correlation of stroke volume (SV), cardiac output (CO), for each individual animal across the four phases of the estrous cycle.



In the analysis of Pulse wave Doppler parameters for the pulmonary artery, aortic outflow, mitral valve, and tricuspid valve, no significant differences were observed across the measurements (Table 4). Additionally, when evaluating non-invasive blood pressure

measurements, no significant variations were detected between the different estrous phases (Table 5).

Table 4: Pulse wave doppler parameters for PA, Ao, MV, and TV. *Values are means ± SD*

Pulmonary Artery (PA) and Aortic Outflow (Ao) Parameters				
	Proestrus (n = 9)	Estrus (n = 9)	Metestrus (n = 8)	Diestrus (n = 9)
PA VTI (mm)	26.64 ± 3.51	26.17 ± 5.05	25.79 ± 4.45	23.69 ± 2.16
PA Mean Velocity (mm/s)	-371.59 ± 42.03	-323.4 ± 52.85	-364.79 ± 85.96	-325.55 ± 27.91
PA Peak Velocity (mm/s)	-650.17 ± 64.75	-569.32 ± 110.91	-620.20 ± 114.36	-576.06 ± 47.73
Ao VTI	29.28 ± 6.82	27.55 ± 4.38	27.67 ± 5.44	26.20 ± 2.98
Ao Mean Velocity (mm/s)	476.20 ± 120.10	459.41 ± 69.5	449.94 ± 93.95	422.72 ± 56.73
Ao Peak Velocity (mm/s)	785.01 ± 173.14	775.32 ± 116.62	743.41 ± 139.17	720.15 ± 91.68
Mitral Valve (MV) and Tricuspid Valve (TV) Parameters				
AET (ms)	48.57 ± 4.29	45.18 ± 5.61	51.84 ± 12.16	45.35 ± 4.82
IVCT (ms)	17.74 ± 4.11	13.74 ± 4.59	12.49 ± 3.42	13.69 ± 3.39
IVRT (ms)	16.10 ± 4.59	17.34 ± 2.80	15.94 ± 3.70	16.77 ± 2.39
MV A (mm/s)	353.90 ± 121.01	304.18 ± 68.57	390.38 ± 71.16	327.850± 101.63
MV E (mm/s)	499.08 ± 80.27	453.39 ± 54.55	509.72 ± 90.27	487.50 ± 47.85
LV MPI IV	0.73 ± 0.17	0.70 ± 0.19	0.70 ± 0.22	0.69 ± 0.11

Table 5: Non-Invasive Longitudinal BP Measurements

	Proestrus	Estrus	Metestrus	Diestrus
	n = 9	n = 9	n = 8	n = 9
Systolic BP	137.74 ± 16.40	130.45 ± 20.75	141.03 ± 29.28	133.85 ± 11.08
Diastolic BP	105.44 ± 16.54	99.35 ± 21.56	109.58 ± 27.97	104.06 ± 10.61
Mean BP	115.92 ± 16.47	109.35 ± 21.23	119.60 ± 28.23	114.06 ± 10.67

Terminal

At the terminal timepoint, the average body weight of animals in proestrus and diestrus were 25.66 ± 3.01 g and 28.00 ± 2.92 g, respectively. The weights of the whole heart

(0.14 ± 0.01 g vs. 0.13 ± 0.01 g), right ventricular free wall (0.02 ± 0.01 vs. 0.02 ± 0.01 g) and left ventricular free wall and septum (0.09 ± 0.01 g vs. 0.09 ± 0.01 g) were not significantly different (Table 6). However, when comparing percent uterus weight: body weight, we see a significant difference between the two phases with proestrus at 0.41 ± 0.03 % uterus weight: body ratio and diestrus at 0.36 ± 0.03 % uterus weight: body ratio (Fig 14A). Interestingly, the uterus during proestrus appeared pinker and fuller, while in diestrus, it was observed to be yellow and thinner (Fig 14B).

Table 6: Body and heart chamber weight ratios for Proestrus vs Diestrus. Values are means ± SD;

	Proestrus (n = 5)	Diestrus (n = 4)
Age	6 months	6 months
Body Mass (g)	25.66 ± 3.01	28.00 ± 2.92
Uterus (g)	0.11 ± 0.01	0.10 ± 0.01
Whole Heart (g)	0.14 ± 0.01	0.13 ± 0.01
LV + S (g)	0.09 ± 0.01	0.09± 0.01
RV (g)	0.02 ± 0.01	0.02 ± 0.01

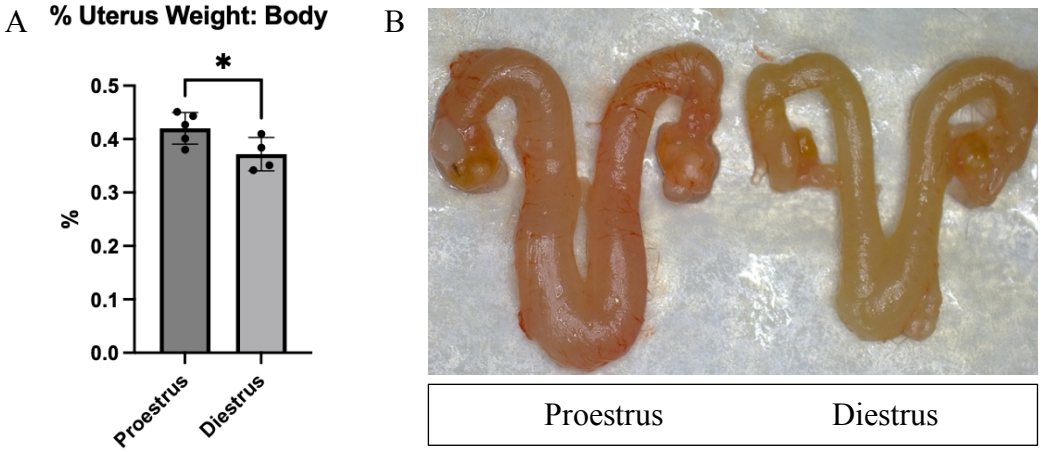


*Figure 14: A) Comparing percent uterus weight: body weight, Proestrus 0.41 ± 0.03 vs. Diestrus 0.36 ± 0.03 % uterus weight: body ratio, *P < 0.05 B) Observation of uterus size and color between proestrus and diestrus time point.*

From our invasive hemodynamic measurements, we observed that heart rate remained consistent across the entire collection period for all animals, regardless of whether they were in proestrus or diestrus. Notably, there was a significant difference in ejection fraction between these two phases, with a p-value of 0.03. However, no significant differences were found between the phases for other measured parameters.

Table 7: Invasive hemodynamic measurements were obtained in n = 5 for proestrus and n = 4 for diestrus.

	Proestrus (n = 5)	Diestrus (n = 4)
HR (bpm)	618.82 ± 26.83	611.68 ± 48.36
ESP (mmHg)	73.98 ± 14.63	64.45 ± 17.74
EDP (mmHg)	4.32 ± 0.68	3.71 ± 0.48
ESV (uuL)	11.92 ± 2.25	22.11 ± 9.50
EDV (uL)	18.32 ± 3.77	31.61 ± 13.83
SW (*)	572.92 ± 179.17	625.71 ± 274.37
CO (/min)	4627.21 ± 1076.05	6077.25 ± 1841.77
SV	7.51 ± 1.87	10.08 ± 3.52
EF (%)	39.51 ± 2.58*	32.97 ± 4.65*
dP/dt max (/s)	9172.21 ± 1930.96	8404.51 ± 3992.02
dP/dt min (/s)	-7029.41 ± 1860.17	-6250.25 ± 2177.18
Tau (ms)	5.94 ± 0.81	6.47 ± 1.04
Ea (/)	10.73 ± 3.23	7.91 ± 4.65
Vmax (Pmean)	80.38 ± 11.93	69.16 ± 17.81
Vmin (Pdev)	2.22 ± 0.73	2.13 ± 1.17
Pmax	30.87 ± 6.76	25.63 ± 8.75
Pmin	78.16 ± 11.73	67.03 ± 18.52
PowMax (*/s)	124040 ± 47800.97	212425 ± 134208.02
dV/dt max (/s)	2006.61 ± 655.24	4251.51 ± 2950.28
dV/dt min (/s)	-2384.41 ± 704.34	-4321.51 ± 2874.12
P@dV/dt max	50.06 ± 14.65	37.77 ± 21.557
P@dP/dt max	41.15 ± 18.04	35.52 ± 20.68
V@dP/dt max	18.80 ± 4.09	31.42 ± 13.05
V@dP/dt min	11.29 ± 2.31	20.92 ± 9.07

EF was significantly lower (p-value 0.03) during proestrus compared to diestrus. Values are *means ± SD* (*P < 0.05)

3.4 - Discussion

Female sex hormones, specifically estrogen, have been considered cardioprotective [10]. However, research on the role of female sex hormones on cardiac function in premenopausal women is lacking. Historically, female sex was excluded from clinical studies and animal research prompting the NIH Policy on Sex as a Biological Variable in 2015 [2]. This study sought to determine the impact of hormonal fluctuations over the mouse estrous cycle on cardiac function. Our investigation found increased fractional shortening and ejection fraction during proestrus compared to diestrus.

Numerous studies have demonstrated significant variations in myocardial parameters like aortic stiffness, cardiac contraction, and calcium transients associated with differing estrogen levels [5, 20, 21]. In our study, we observed a higher average fractional shortening during estrus compared to diestrus. This observation is consistent with MacDonald et al., who reported that fractional shortening during estrus, characterized by elevated estrogen levels, is approximately twice as high as during diestrus, when estrogen levels are lower [5]. Additionally, Kwissa et al. observed significantly shorter left ventricular ejection times during the mid-luteal phase compared to the late follicular phase of the menstrual cycle in human women [20]. Similarly, our study found that cardiac contractility, measured by fractional shortening, increased during the proestrus phase, which is also characterized by high estrogen levels. As the cycle progresses, our data show a general downward trend in both fractional shortening (FS) and ejection fraction (EF), correlating with decreasing estrogen levels and rising progesterone.

Chapter 4: Conclusion

In conclusion, our investigation sheds light on the intricate relationship between the estrous cycle and cardiac dynamics. By connecting our major findings to existing literature and emphasizing the role of estrogen, we advocate for a refined approach to cardiovascular research that considers both sex and estrous cycle phases which may help improve timing for medical interventions in premenopausal women and prompt animal researchers to report estrous phase as a variable within the study.

Chapter 5: Future Directions

Hormone concentration throughout estrous cycle

Even though phases of estrous cycle were identified via vaginal cytology a second form of confirmation should still be implemented. It has been recommended that studies measuring steroid hormones, such as 17β-estradiol and progesterone, utilize mass spectrometry-based assays to guarantee specificity and reproducibility [22]. Therefore, I propose a project using Liquid Chromatography Mass Spectrometry (LC-MS) to quantify hormone concentrations in serum samples collected at terminal time points throughout the estrous cycle. I hypothesize that there will be a correlation between 17β-estradiol levels and fluctuations in ejection fraction and fractional shortening.

Left ventricular function and pressure flow measurements throughout the estrous cycle

Although we successfully collected ventricular function and pressure flow measurement during proestrus and diestrus (n = 5 and n = 4, respectively), a larger sample size is necessary to detect more significant differences between these phases. I propose expanding the study to include additional subjects and to collect data for the estrus and

metestrus phases as well. I predict this approach will provide comprehensive data on how pressure and ventricular function vary throughout each phase of the estrous cycle.

Induce regular cycling throughout estrous cycle

One limitation of our study was that the female mice did not display regular estrous cycles, likely due to the inhibitory effect of female pheromones, known as the Lee-Boot effect [23]. For future studies, I propose inducing regular cycling by exposing mice to bedding collected from the cages of young adult male mice, as MacDonald et al. demonstrated [5]. I expect this approach will improve the timing of all phases, particularly metestrus, which is challenging to capture with natural cycling.

Reference

1. Heather LC, Hafstad AD, Halade GV, Harmancey R, Mellor KM, Mishra PK, Mulvihill EE, Nabben M, Nakamura M, Rider OJ, Ruiz M, Wende AR, Ussher JR. Guidelines on models of diabetic heart disease. Am J Physiol Heart Circ Physiol. 2022 323(1):H176-H200. http://dx.doi.org/10.1152/ajpheart.00058.2022. https://www.ncbi.nlm.nih.gov/pubmed/35657616. https://www.ncbi.nlm.nih.gov/pmc/articles/PMC9273269.
2. Clayton JA, Collins FS. Policy: NIH to balance sex in cell and animal studies. Nature. 2014 509(7500):282-3. http://dx.doi.org/10.1038/509282a. https://www.ncbi.nlm.nih.gov/pubmed/24834516. https://www.ncbi.nlm.nih.gov/pmc/articles/PMC5101948.
3. Lindsey ML, LeBlanc AJ, Ripplinger CM, Carter JR, Kirk JA, Hansell Keehan K, Brunt KR, Kleinbongard P, Kassiri Z. Reinforcing rigor and reproducibility expectations for use of sex and gender in cardiovascular research. Am J Physiol Heart Circ Physiol. 2021 321(5):H819-H24. http://dx.doi.org/10.1152/ajpheart.00418.2021. https://www.ncbi.nlm.nih.gov/pubmed/34524922.
4. Kehmeier MN, Bedell BR, Cullen AE, Khurana A, D'Amico HJ, Henson GD, Walker AE. In vivo arterial stiffness, but not isolated artery endothelial function, varies with the mouse estrous cycle. Am J Physiol Heart Circ Physiol. 2022 323(6):H1057-H67. http://dx.doi.org/10.1152/ajpheart.00369.2022. https://www.ncbi.nlm.nih.gov/pubmed/36240435. https://www.ncbi.nlm.nih.gov/pmc/articles/PMC9678414.
5. MacDonald JK, Pyle WG, Reitz CJ, Howlett SE. Cardiac contraction, calcium transients, and myofilament calcium sensitivity fluctuate with the estrous cycle in young adult female mice. Am J Physiol Heart Circ Physiol. 2014 306(7):H938-53. http://dx.doi.org/10.1152/ajpheart.00730.2013. https://www.ncbi.nlm.nih.gov/pubmed/24464757.
6. Auta T, Hassan AT. Alteration in oestrus cycle and implantation in Mus musculus administered aqueous wood ash extract of Azadirachta indica (neem). Asian Pac J Reprod. 2016 5(3):188-92. http://dx.doi.org/10.1016/j.apjr.2016.03.003.
7. Ajayi AF, Akhigbe RE. Staging of the estrous cycle and induction of estrus in experimental rodents: an update. Fertil Res Pract. 2020 6(1):5. http://dx.doi.org/10.1186/s40738-020-00074-3. https://www.ncbi.nlm.nih.gov/pubmed/32190339. https://www.ncbi.nlm.nih.gov/pmc/articles/PMC7071652.
8. Cora MC, Kooistra L, Travlos G. Vaginal cytology of the laboratory rat and mouse: Review and criteria for the staging of the estrous cycle using stained vaginal smears. Toxicol Pathol. 2015 43(6):776-93. http://dx.doi.org/10.1177/0192623315570339. https://www.ncbi.nlm.nih.gov/pubmed/25739587.
9. Felicio LS, Nelson JF, Finch CE. Longitudinal studies of estrous cyclicity in aging C57BL/6J mice: II. Cessation of cyclicity and the duration of persistent vaginal cornification 1. Biol Reprod. 1984 31(3):446-53. http://dx.doi.org/10.1095/biolreprod31.3.446.
10. Aryan L, Younessi D, Zargari M, Banerjee S, Agopian J, Rahman S, Borna R, Ruffenach G, Umar S, Eghbali M. The role of estrogen receptors in cardiovascular disease. Int J Mol Sci. 2020 21(12):4314. http://dx.doi.org/10.3390/ijms21124314.

https://www.ncbi.nlm.nih.gov/pubmed/32560398.
https://www.ncbi.nlm.nih.gov/pmc/articles/PMC7352426.
11. Byers SL, Wiles MV, Dunn SL, Taft RA. Mouse estrous cycle identification tool and images. PLoS One. 2012 7(4):e35538. http://dx.doi.org/10.1371/journal.pone.0035538. https://www.ncbi.nlm.nih.gov/pubmed/22514749. https://www.ncbi.nlm.nih.gov/pmc/articles/PMC3325956.
12. Tanaka N, Dalton N, Mao L, Rockman HA, Peterson KL, Gottshall KR, Hunter JJ, Chien KR, Ross J, Jr. Transthoracic echocardiography in models of cardiac disease in the mouse. Circulation. 1996 94(5):1109-17. http://dx.doi.org/10.1161/01.cir.94.5.1109. https://www.ncbi.nlm.nih.gov/pubmed/8790053.
13. Gao S, Ho D, Vatner DE, Vatner SF. Echocardiography in Mice. Current Protocols in Mouse Biology. 2011. http://dx.doi.org/10.1002/9780470942390.mo100130.
14. Philip JL, Murphy TM, Schreier DA, Stevens S, Tabima DM, Albrecht M, Frump AL, Hacker TA, Lahm T, Chesler NC. Pulmonary vascular mechanical consequences of ischemic heart failure and implications for right ventricular function. Am J Physiol Heart Circ Physiol. 2019 316(5):H1167-H77. http://dx.doi.org/10.1152/ajpheart.00319.2018.
15. Stanhewicz AE, Wenner MM, Stachenfeld NS. Sex differences in endothelial function important to vascular health and overall cardiovascular disease risk across the lifespan. Am J Physiol Heart Circ Physiol. 2018 315(6):H1569-H88. http://dx.doi.org/10.1152/ajpheart.00396.2018. https://www.ncbi.nlm.nih.gov/pubmed/30216121. https://www.ncbi.nlm.nih.gov/pmc/articles/PMC6734083.
16. Ryczkowska K, Adach W, Janikowski K, Banach M, Bielecka-Dabrowa A. Menopause and women's cardiovascular health: is it really an obvious relationship? Arch Med Sci. 2023 19(2):458-66. http://dx.doi.org/10.5114/aoms/157308. https://www.ncbi.nlm.nih.gov/pubmed/37034510. https://www.ncbi.nlm.nih.gov/pmc/articles/PMC10074318.
17. Reed BG, Carr BR, Feingold KR, Anawalt B, Blackman MR, Boyce A, Chrousos G, Corpas E, De Herder WW, Dhatariya K, Dungan K, Hofland J, Kalra S, Kaltsas G, Kapoor N, Koch C, Kopp P, Korbonits M, Kovacs CS, Kuohung W, Laferrère B, Levy M, McGee EA, McLachlan R, New M, Purnell J, Sahay R, Shah AS, Singer F, Sperling MA, Stratakis CA, Trence DL, Wilson DP. The Normal Menstrual Cycle and the Control of Ovulation. Dartmouth (MA: MDText.com, Inc; 2000.
18. Moran VH, Leathard HL, Coley J. Cardiovascular functioning during the menstrual cycle. Clin Physiol. 2000 20(6):496-504. http://dx.doi.org/10.1046/j.1365-2281.2000.00285.x. https://www.ncbi.nlm.nih.gov/pubmed/11100398.
19. Martin D, Timmins K, Cowie C, Alty J, Mehta R, Tang A, Varley I. Injury incidence across the menstrual cycle in international footballers. Front Sports Act Living. 2021 3:616999. http://dx.doi.org/10.3389/fspor.2021.616999. https://www.ncbi.nlm.nih.gov/pubmed/33733235. https://www.ncbi.nlm.nih.gov/pmc/articles/PMC7956981.
20. Kwissa M, Krauze T, Mitkowska-Redman A, Banaszewska B, Spaczynski RZ, Wykretowicz A, Guzik P. Cardiovascular function in different phases of the menstrual cycle in healthy women of reproductive age. J Clin Med. 2022 11(19):5861. http://dx.doi.org/10.3390/jcm11195861.

21. Kehmeier MN, Bedell BR, Cullen AE, Khurana A, D'Amico HJ, Henson GD, Walker AE. In vivo arterial stiffness, but not isolated artery endothelial function, varies with the mouse estrous cycle. American Journal of Physiology-Heart and Circulatory Physiology. 2022 2024/04/14;323(6):H1057-H67. https://doi.org/10.1152/ajpheart.00369.2022.
22. Handelsman DJ, Wartofsky L. Requirement for mass spectrometry sex steroid assays in the Journal of Clinical Endocrinology and Metabolism. J Clin Endocrinol Metab. 2013 98(10):3971-3. http://dx.doi.org/10.1210/jc.2013-3375.
23. Dominic CJ. Pheromonal mechanisms regulating mammalian reproduction. Gen Comp Endocrinol. 1969 2:260-7. http://dx.doi.org/10.1016/0016-6480(69)90036-7.